*Food Bioengineering*

WILEY

Food Bioengineering

RESEARCH ARTICLE OPEN ACCESS

# Mechanical Properties of Polylactic Acid Nanofiber Films Reinforced by Modified Cellulose Nanocrystals

Chaoqiao Zhu[1,2] | Ming Tian[1,2] | Dequan Zhang[2] | Qingfeng Yang[2] | Debao Wang[2] | Simin Fan[2,3] | Xin Li[2] | Wei Yang[4] | Chengli Hou[1,2]

[1]College of Food Science and Engineering, Shanxi Agricultural University, Taigu, China | [2]Institute of Food Science and Technology, Chinese Academy of Agricultural Sciences, Key Laboratory of Agro-products Quality and Safety Control in Storage and Transport Process, Ministry of Agriculture and Rural Affairs, Beijing, China | [3]Laboratory of Biomass and Green Technologies, Gembloux Agro-Bio Tech, University of Liège, Gembloux, Belgium | [4]Sunrise Material Co. Ltd, Jiangyin, China

**Correspondence:** Chengli Hou (houchengli@caas.cn)

**Received:** 22 December 2024 | **Revised:** 19 January 2025 | **Accepted:** 2 February 2025

**Funding:** This work was supported by the Major Science and Technology Project of Yunnan Province (No.202102AE090039).

**Keywords:** active packaging | cellulose nanocrystals | electrostatic spinning | esterification reaction | polylactic acid

## ABSTRACT

In this study, the surface of cellulose nanocrystals was first modified with citric acid, and the resultant modified cellulose nanocrystals (MCNC) were subsequently utilized as a reinforcement phase for polylactic acid (PLA). Findings indicated that MCNC interacted with PLA through hydrogen bonding, resulting in improved thermal stability, mechanical properties, and surface hydrophobicity of PLA nanofiber films. Specifically, the thermal degradation temperature, tensile strength, elongation at break, and contact angle of the nanofiber films increased by 19°C, 30.04%, 49.11%, and 11.22°, respectively, with a 3% addition of MCNC. Subsequently, utilizing PLA/MCNC as the base material and kaempferol as the active ingredient, a preliminary exploration into its potential as an active packaging material was carried out. When the addition amount of kaempferol was 10%, the DPPH and ABTS free radical scavenging ability of the nanofiber film reached more than 90%, demonstrating its application potential as an active packaging material. These results offer a promising strategy for the effective dispersion of CNC within PLA matrices, thereby expanding the potential applications of PLA in the field of active packaging.

## 1 | Introduction

Petroleum-derived plastics have emerged as essential materials in the packaging sector, owing to their cost-effectiveness and outstanding performance (Karimi Sani et al. 2023; Li et al. 2024). Nevertheless, the persistent accumulation of plastic waste increasingly threatens both ecosystems and human health (Li et al. 2024). Given this, there is an urgent need to change the focus of research and development to high-performance, renewable, biodegradable new packaging materials.

Polylactic acid (PLA) is a renewable and biodegradable polymer material with the potential to replace traditional commercial plastics in various applications (Azka et al. 2024). PLA is synthesized from lactic acid or lactide, and these precursor materials are mainly fermented from renewable plant resources such as sugarcane, potatoes, and corn (Malbos et al. 2024; Yanat et al. 2023). Besides its renewable and degradable properties, PLA exhibits excellent processing performance and high transparency (Gazquez-Navarro et al. 2024). Notably, the US Food and Drug Administration (FDA) has classified PLA as Generally Regarded As Safe (GRAS) and approved it for use in food packaging

(Gao et al. 2023). Although PLA possesses numerous advantages compared with petroleum-based polymers, it still has deficiencies in thermal stability and toughness, which to some extent restricts the feasibility of its commercial application (N'a et al. 2023). Therefore, further research is necessary to overcome these limitations, with the use of nanofillers to enhance PLA's mechanical properties being a promising solution (Niu et al. 2018).

Cellulose nanocrystals (CNC), derived from natural cellulose, not only have a wide range of raw materials but also possess superior characteristics such as high strength, modulus, crystallinity, and low toxicity (Kataria et al. 2023; Liu et al. 2024; Zhou et al. 2021). As a reinforcing material, CNC can enhance the mechanical and thermal stability of PLA without sacrificing its environmental benefits (Chaturvedi et al. 2023; Niu et al. 2022). However, the abundant hydroxyl groups on the surface of CNC exhibit strong hydrophilicity, which hinders its uniform dispersion within the hydrophobic PLA matrix, leading to a reduction in the enhancement effect (Dhali et al. 2022). Therefore, modifying the CNC surface is essential to improve its dispersibility in the PLA composite. Esterification modification, which involves replacing the hydroxyl groups on the surface with ester groups, is a key approach for surface modification of CNC (Thompson et al. 2022). With growing concerns about production safety and environmental impact, eco-friendly and nontoxic esterification reactions have emerged as a significant research focus. In this context, the use of citric acid, a naturally occurring organic acid, for esterifying CNCs aligns with people's aspirations for health and safety (Lin et al. 2022).

In PLA-based packaging materials, nanofillers are commonly incorporated to enhance their mechanical properties, while active substances are added to impart specific functionalities. This study aims to modify CNC using citric acid to achieve uniform dispersion in the PLA matrix. The potential application of modified cellulose nanocrystals (MCNC) as a reinforcing material for PLA was then explored. Subsequently, a nanofiber film was prepared by mixing kaempferol as the active substance with PLA and MCNC, and the effect of the matrix on the antioxidant capacity was evaluated. With the expectation of providing a reference for the research and development of PLA-based active packaging.

## 2 | Materials and Methods

### 2.1 | Materials

PLA (molecular weight :80,000, particle size: 3 mm) and N, N-dimethylformamide (analytical reagent, ≥ 99.5%) were provided by Macklin Biochemical Co. Ltd (Shanghai, China). CNC powder was acquired from Zhengzhou Feiman Biotechnology Co. Ltd. (Zhengzhou, China). Citric acid was bought from Tianjin Zhiyuan Chemical Reagent Co. Ltd. (Tianjin, China). Dichloromethane was purchased from Beijing Tongguang Fine Chemical Co. Ltd. (Beijing, China). kaempferol and ABTS were acquired from Yuanye Biotechnology Co. Ltd. (Shanghai China).

### 2.2 | Surface Modification of CNC

MCNC were prepared using the method outlined by Lin et al. (2022) with some modifications. As demonstrated in Video S1, a mixture of citric acid (1.25 g) and a 0.50% CNC suspension (50.00 g) was placed in a round flask. A distillation system was then installed, and the mixture was stirred for 7 h at 130°C in an oil bath. At the end of the reaction, the mixture was dialyzed with pure water to pH neutral to eliminate unreacted citric acid. Finally, the mixture was freeze-dried to obtain the MCNC. Figure 1a illustrates the possible reaction mechanism between CNC and citric acid, where the hydroxyl group of CNC reacts with the carboxyl group of citric acid to form an ester bond.

### 2.3 | Preparation of PLA/MCNC Nanofiber Films

Figure 1b illustrates the preparation process of the nanofiber film and the potential reaction mechanisms of MCNC and PLA. When MCNC was incorporated into PLA, potential interactions occurred between its surface functional groups and the PLA matrix, thereby enhancing the reinforcement effect of the PLA. Specifically, a solution of dichloromethane (DCM) and *N,N*-dimethylformamide (DMF) in a 7:3 volume ratio was mixed with a precise weight of PLA particles. This mixture underwent magnetic stirring at room temperature until the complete dissolution of the particles. Subsequently, varying ratios of CNC and MCNC were incorporated into the PLA solution. Continuous stirring for 12 h ensured thorough dissolution. The spinning solution was obtained by ultrasonic degassing for 20 min at 40 Hz and 360 W. The total solute mass fraction was maintained at 12% (w/v), with the mass fractions of CNC and MCNC at 1%, 3%, and 5% (w/w) of the overall mass. These solutions were noted as PLA, PLA/CNC1%, PLA/CNC3%, PLA/CNC5%, PLA/MCNC1%, PLA/MCNC3%, and PLA/MCNC5%. The nanofiber films were prepared using the ET-2535 electrospinning equipment (Beijing Yongkang Technology Development Co. Ltd., China). The spinning solutions were filled into a 5 mL syringe fitted with an 18 G needle. The following were the precise spinning parameters: temperature: 25 ± 2°C; relative humidity: 40%–50%; reception distance: 15 cm; advance speed: 0.2 mm/min; roller drum collecting speed: 30 r/min; moving distance: 60 mm; voltage: 15 kV.

### 2.4 | Preparation of PMK Nanofiber Films

A total of 1.16 g of PLA and 0.04 g of MCNC were sufficiently dissolved in 10 mL of DCM and DMF mixed solution. To the above solution, various amounts of kaempferol—0%, 1%, 3%, 5%, and 10% (w/w)—were added and stirred for 12 h, after which the mixture was sonicated for 20 min at 40 Hz 360 W and marked as PMK0, PMK1, PMK3, PMK5, and PMK10 according to the content of kaempferol. The preparation of the nanofiber films was consistent with Section 2.3.

### 2.5 | Morphology

The transmission electron microscope (TEM, H-7500, Hitachi, Japan) was used to investigate the morphology of the CNC and MCNC. An aqueous solution containing 0.05% CNC and MCNC was placed in a carbon-coated copper grid and observed after drying at room temperature (Sung et al. 2017).

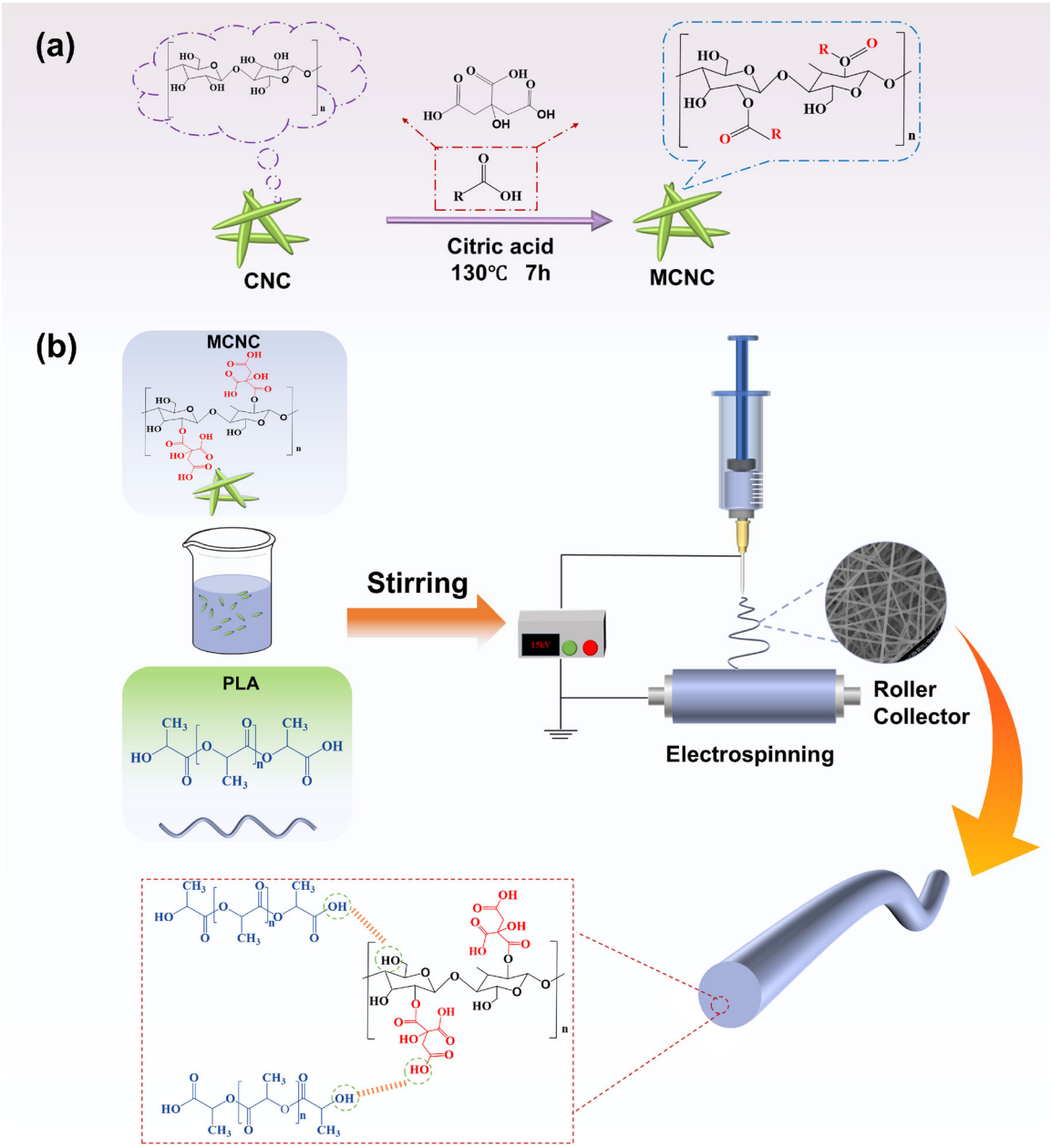


**FIGURE 1** | Schematic diagram of the CNC esterification reaction mechanism with citric acid (a), and the preparation process of nanofiber films and possible reaction mechanism of MCNC and PLA (b).

A cold-field emission scanning electron microscope (SEM, SU8010, Hitachi, Japan) was used to observe the microscopic structure of the nanofiber films. The films were fixed on the conductive adhesive and observed after gold spraying. The diameter distribution of nanofibers was determined by examining around 100 fiber threads using Image J software (Zhu et al. 2024).

### 2.6 | FTIR

The FTIR spectra of CNC, MCNC, and nanofiber films were acquired using an FTIR spectrometer with an ATR accessory (TENSOR27, Germany) within a scanning range of 4000–400 $cm^{-1}$ with 64 scans (Ertan et al. 2023).

### 2.7 | XRD

The materials' crystallization was examined using the X-ray diffractometry (Rigaku Ultima IV, Japan). The scanning rate was 5°/min, and the 2θ range was 5°–60° (Yang et al. 2023).

### 2.8 | Thermal Stability

The thermal stability of all the specimens was evaluated through thermogravimetric (TG) analysis (Perkin Elmer TG/DTA, USA). Samples with a weight ranging from 3 to 5 mg were heated from 30°C to 500°C at a rate of 10°C/min in a nitrogen ($N_2$) atmosphere (Yun et al. 2024).

### 2.9 | Mechanical Properties

The films were divided into strips with dimensions of (60.00 mm × 10.00 mm). The tensile strength (TS) and elongation at break (EAB) of these strips were measured using a TA-XT-PLUS (Stable Micro Systems Company, US) referring to previous studies (Fan et al. 2023). The film's thickness was determined at five distinct sites using a vernier caliper, and subsequently, the mean value was computed. The instrument was set up with the following measurement parameters: an original distance of 25.00 mm and a test speed of 50.00 mm/min. A total of five replicates were conducted.

### 2.10 | Water Contact Angle (WCA)

The WCA of the nanofiber films was determined using an SZ-CAMC32 instrument (Shanghai Xuan Zhun Co. Ltd., China). The video of 5 min from the beginning of the droplet's low fall was recorded, and the instantaneous images of 0 min, 1 min, and 5 min were intercepted by continuous shooting mode to measure the contact angle.

### 2.11 | Water Vapor Permeability (WVP)

The WVP of nanofiber films was determined using a previous method (Wu et al. 2023). The nanofiber films were fixed in 50.00 mL centrifuge tubes (inner diameter 27 mm) that contained 20.00 ± 0.05 g of dried silica gel. The starting mass was measured and subsequently transferred to a controlled environment with a consistent temperature of 25°C and a relative humidity of 75%. The process of weighing was conducted at 24-h intervals until Day 7. The calculation formula for WVP was as follows:

$$\mathrm{WVP} = \frac{\Delta m \times d}{S \times T \times \Delta P} (\mathrm{g\ m^{-1}\ d^{-1}\ kPa^{-1}}).$$

The variables in the formula are as follows: $\Delta m$ represents the mass increase of the centrifuge tubes (g), $d$ represents the thickness of the films (m), $T$ represents the test time (d), $S$ represents the experimental area of the films ($m^2$), and $\Delta P$ represents the pressure difference between two sides of the films (kPa).

### 2.12 | Antioxidant Properties

The antioxidant activity of the films was determined using the DPPH free radical scavenging assay kit (BC4750, Solarbio, Beijing, China). The measurement and calculation were performed in accordance with the kit instructions.

The ABTS radical scavenging ratio was evaluated according to the modified method (Gulzar et al. 2022). Equal volumes of ABTS (7.4 mM) and potassium persulfate (2.6 mM) were blended and reacted for 12 h in the dark. Thereafter, it was diluted with ethanol until an absorbance value of 1.1 was attained, thereby preparing the ABTS working solution. The 30 mg film samples were placed in 3 ml of 95% ethanol and subjected to a 12 h extraction process. In brief, 190 μL of the ABTS working solution was combined with 10 μL of the sample solution in each well of a 96-well microplate. Subsequently, the microplate was permitted to react under dark conditions for 6 min, and the absorbance was determined at 734 nm using a multifunctional microplate reader (SuPerMax 3000FA, Shanghai Shanpu Biotechnology Co. Ltd., China). The rate of ABTS free radical scavenging was calculated based on the following equation.

$$\text{ABTS scavenging rate } (\%) = \frac{A_{\mathrm{blank}} - (A_{\mathrm{test}} - A_{\mathrm{control}})}{A_{\mathrm{blank}}},$$

$A_{\mathrm{blank}}$ is the working solution + 95% ethanol solution; $A_{\mathrm{test}}$ is the working solution + sample solution; $A_{\mathrm{control}}$ is the sample solution + 95% ethanol solution.

### 2.13 | Statistical Analysis

All results were presented as mean ± standard deviation. Using SPSS (IBM, 26.0), analysis of variance (ANOVA) was carried out, and multiple comparisons were carried out using Duncan's test. Differences were considered significant at $p < 0.05$. All figures were generated using Origin 2021 software.

## 3 | Results and Discussion

### 3.1 | Morphology Analysis

The TEM images of CNC and MCNC are shown in Figure 2. CNC exhibited a typical rod-like shape accompanied by significant aggregation (Figure 2a), which was attributed to the strong intramolecular hydrogen bonds within the CNC (Ojogbo et al. 2025). Following modification with citric acid, the rod-like shape was preserved without apparent aggregation (Figure 2b). The introduction of citric acid to the CNC surface notably reduced aggregation, which may help to improve the composite film's performance. In addition, the contour part of the MCNC was blurry, which may have resulted from the partial dissolution of the cellulose molecules during esterification (Lin et al. 2011).

SEM images, fiber diameter distribution, and an illustrative diagram of the nanofiber film were shown in Figure 3. All nanofiber films exhibited a typical porous network structure, devoid of beads or spindles. The PLA fibers displayed a smooth surface and a uniform diameter of approximately 1.10 ± 0.20 μm, with overall good morphology. Upon the addition of CNC and MCNC, the fiber surface remained smooth, with no discernible aggregation of CNC or MCNC, indicating that the nanofiber films had evenly encapsulated CNC and MCNC. Furthermore, the average diameter of the nanofiber films with CNC and MCNC did not change significantly, ranging from 0.95 μm to 1.09 μm.

### 3.2 | FTIR Analysis

The spectrum for CNC shows a wide and strong peak at 3342 $cm^{-1}$, which was linked to the –OH stretching vibration of

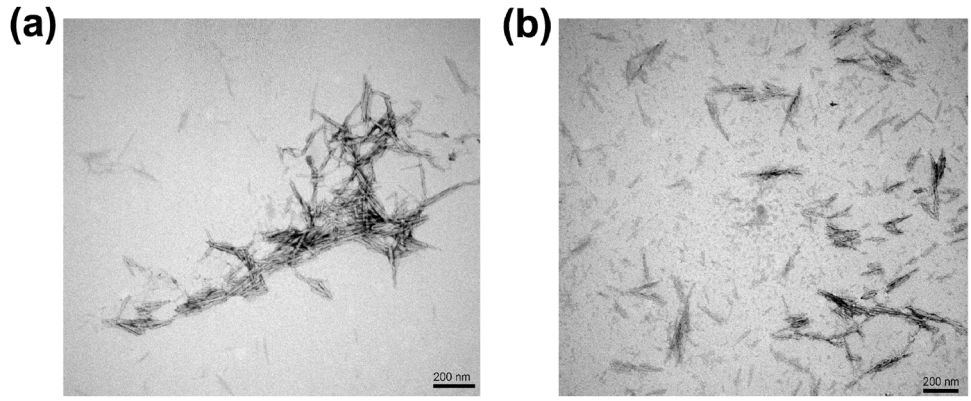


**FIGURE 2** | TEM images of CNC (a) and MCNC (b).

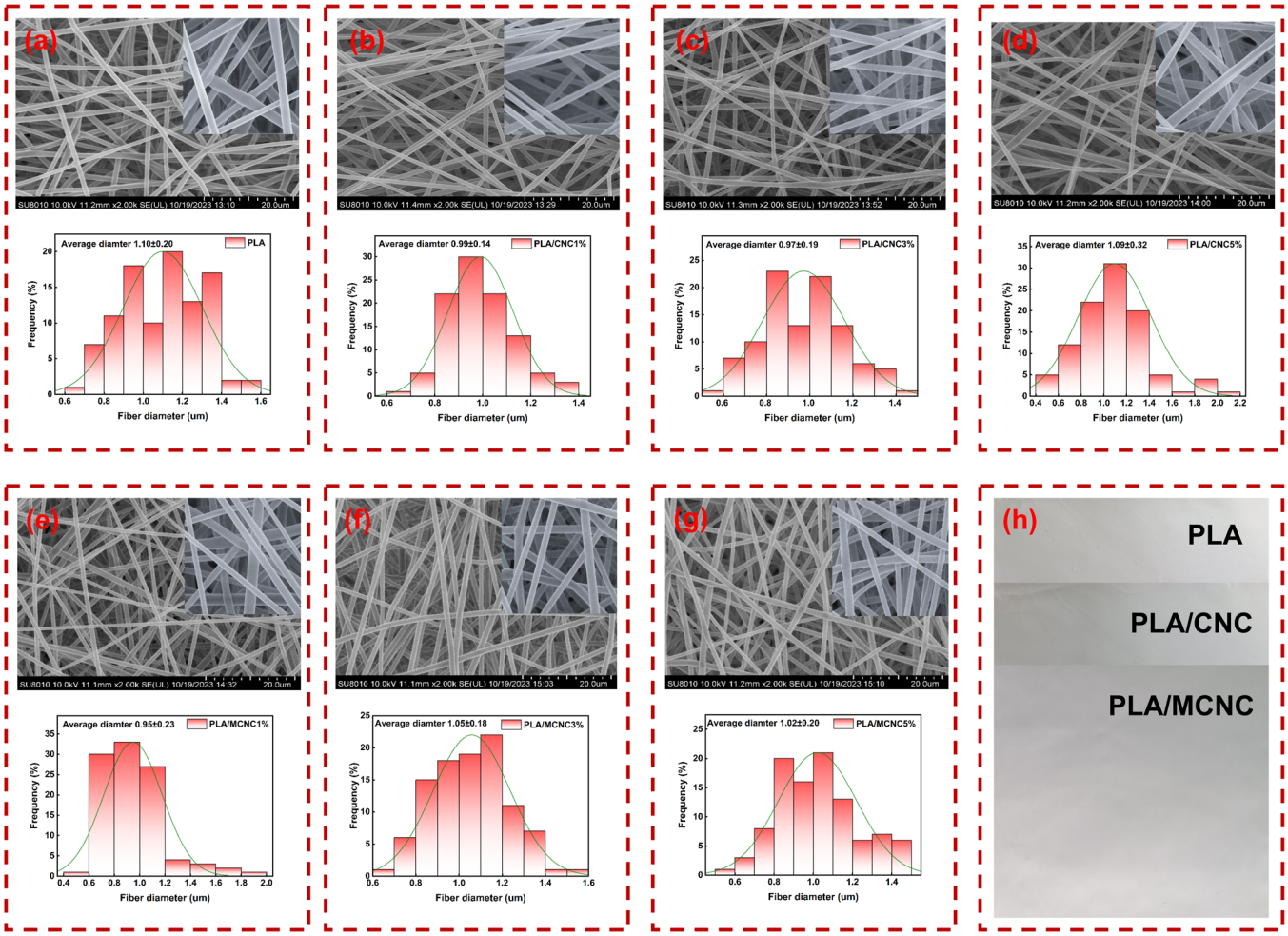


**FIGURE 3** | The SEM images of different films and the corresponding diameter distributions of nanofiber: PLA (a), PLA/CNC1% (b), PLA/CNC3% (c), PLA/CNC5% (d), PLA/MCNC1% (e), PLA/MCNC3% (f), PLA/MCNC5% (g), and optical photographs of different nanofiber films (h).

the intramolecular hydrogen bonding of the CNC (Figure 4a). The peak at 2896 $cm^{-1}$ was attributed to the C–H stretching vibration, whereas the peak at 1642 $cm^{-1}$ was indicative of water molecules adsorbed by cellulose. The 1636 and 1164 $cm^{-1}$ peaks were associated with the bending vibration of C–H and the stretching vibration of C–O–C, respectively (Etale et al. 2024; Khanjanzadeh et al. 2018). In comparison with the CNC spectrum, MCNC exhibited a new peak near 1730 $cm^{-1}$, which was attributed to the stretching vibration of the carbonyl group (C═O) produced from the esterification process. This suggests that the esterification reaction between citric acid and the hydroxyl group on the CNC was successfully carried out (Lin et al. 2022).

As shown in Figure 4b, the characteristic peaks at 2994, 2944, and 1750 $cm^{-1}$ were related to C–H asymmetric, symmetric stretching, and C═O stretching vibration. The characteristic peaks at 1454, 1357, 1184, and 1086 $cm^{-1}$, correspond to C–H asymmetric, symmetric bending, C–O–C, and C–O stretching vibrations,

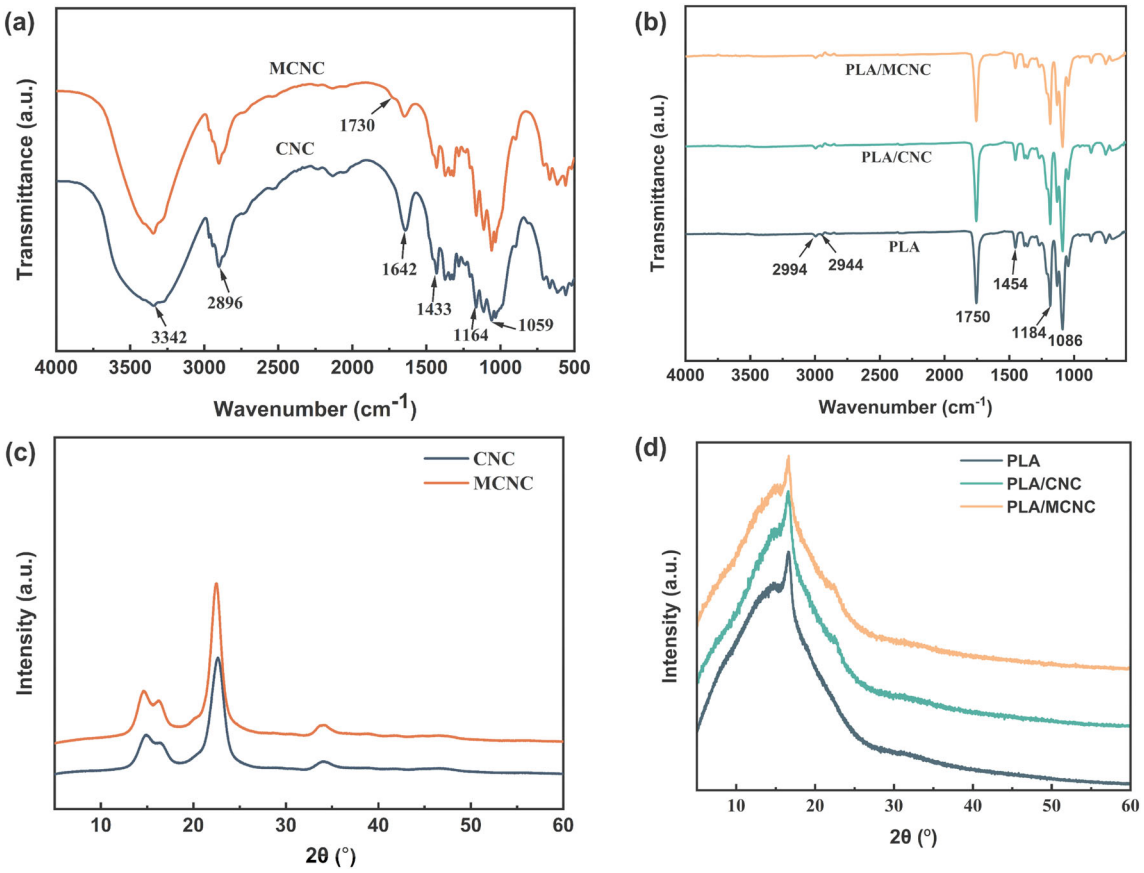


**FIGURE 4** | FTIR spectra of CNC and MCNC (a), and the different nanofiber films (b). X-ray diffraction patterns of CNC and MCNC (c), and the different nanofiber films (d).

respectively (Gao et al. 2023; Mo et al. 2022). These were typical characteristic peaks of PLA. With the addition of CNC and MCNC, no new characteristic peaks or noticeable peak variations were observed, suggesting that no new covalent bonds were formed. Through hydrogen bonding, CNC and MCNC were distributed throughout the PLA matrix (Huang et al. 2023).

### 3.3 | XRD Analysis

The XRD patterns of CNC and MCNC were shown in Figure 4c. The CNC and MCNC exhibited similar diffraction peaks at about $2\theta = 14.88°$, 16.37°, 22.63°, and 34.19°, which corresponded to $(1\bar{1}0)$, (110), (200), and (004) crystal faces, respectively, for the cellulose I structure (Khanjanzadeh et al. 2018). A comparison of the diffraction patterns of CNC and MCNC revealed that the positions of their diffraction peaks were essentially consistent, with only a slight increase in intensity observed. This suggests that the esterification reaction primarily occurred on the surface of the CNC and with no disruption to its crystal structure.

The crystalline structure of nanofiber films was characterized by XRD, as shown in Figure 4d. The PLA showed a characteristic diffraction peak at 16.67°, which was consistent with the findings of Liao et al. (2023). This characteristic peak also appeared in the X-ray diffraction patterns of PLA/CNC and PLA/MCNC, which indicated that CNC and MCNC did not disrupt the crystalline structure of the PLA films. Furthermore, a distinct diffraction peak belonging to CNC appeared at 2θ of 22.66° after the incorporation of CNC and MCNC, which proved that CNC was successfully loaded in the nanofiber films.

### 3.4 | Thermal Analysis

The TG and derivative TG (DTG) curves of CNC and MCNC powder were shown in Figure 5. The thermal weight loss process can be divided into three stages: first, water evaporation (30°C–180°C), followed by the decomposition of CNC chain segments (200°C–370°C), and finally, the decomposition of carbon-containing substances (370°C–500°C) (Figure 5a). In comparison to CNC, MCNC exhibited higher thermal decomposition temperatures and maximum thermal weight loss rate temperatures at 5 wt% and 50 wt% weight loss, with increases of 43°C, 13°C, and 53°C, respectively (Figure 5b). This indicates that MCNC demonstrated superior thermal stability than CNC. This could be the result of the introduction of sulfate groups ($O–SO_3$) during the preparation process, which yields CNC by hydrolysis of sulfuric acid. The thermal stability of the dehydration reaction was lowered by the presence of sulfate groups (Cheran et al. 2024). This phenomenon was also reported by Lin and Dufresne (2014). After modification, the majority of the surface sulfate groups were removed, resulting in an enhancement of the thermal stability of MCNC.

The thermal stability of the nanofiber films was assessed using TG analysis. As shown in Figure 5c, the TG curve of PLA

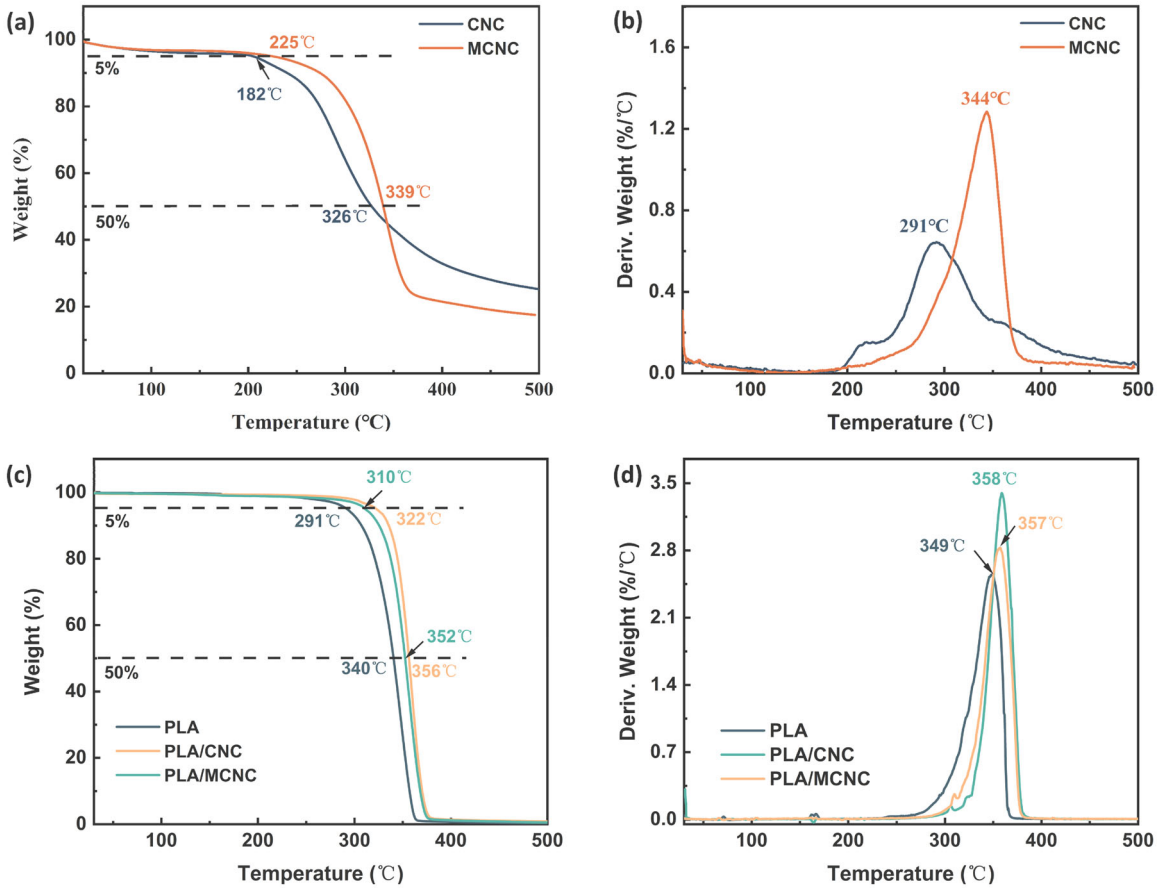


**FIGURE 5** | TG (a) and DTG (b) curves of CNC and MCNC, and TG (c) and DTG (d) curves of the nanofiber films.

showed a single-step degradation with rapid thermal degradation that began at about 290°C, which relates to the thermal degradation of the main chains of PLA (Dhar et al. 2016; Sucinda et al. 2021). The TG curves of the PLA/CNC and PLA/MCNC nanofiber films were basically consistent with those of PLA, and the rapid thermal degradation began at about 322°C and 310°C, respectively. The DTG curve showed that the maximum weight loss rate $T_{(max)}$ temperature of PLA was 349°C. After loading with CNC and MCNC, $T_{(max)}$ increased to 358°C and 357°C, respectively (Figure 5d). This indicates that the entanglement of PLA molecular chains with CNC and MCNC molecular chains, which raises the crosslinking density and restricts the thermal motion of PLA molecular chains, improves the heat resistance of PLA/CNC and PLA/MCNC nanofiber films. This means that CNC and MCNC contribute to inhibiting the thermal degradation of PLA.

## 3.5 | Mechanical Properties Analysis

The variations of the TS and EAB of nanofiber films with different CNC and MCNC content were shown in Figure 6a,b. It was claimed that CNC significantly affects PLA films TS (Sung et al. 2017). Similar outcomes were observed in this work: TS increased dramatically to 3.11 MPa when CNC was introduced to PLA nanofiber films, compared with the control group (PLA 2.23 MPa). In contrast, EAB did not change considerably, which might be explained by the rigidity of CNC itself. The diagram of the tensile process of the PLA/MCNC3% nanofiber films is shown in Figure 6c. It could be seen that the nanofiber film has good ductility, which was confirmed by the analysis of the EAB results. PLA nanofiber films with MCNC added exhibited higher EAB than both pure PLA (109.82%) and other nanofiber films, particularly increased by 49.11% at PLA/MCNC3% (163.75%). This result could be explained by the plasticizing effect of citric acid molecules grafted on CNC. Studies have shown that citric acid has a plasticizing effect on the film (Wahlström et al. 2024). The increase in MCNC proportions typically resulted in a decrease in the EAB of the nanofiber films. This could be attributed to excessive MCNC agglomerates on the surface of the fibers, which resulted in stress concentration and the strength of interactions among molecules being reduced.

## 3.6 | Water Vapor Permeability and Contact Angle Test Analysis

The WVP was a significant parameter for packaging materials, which directly impacts the quality of packaging products. As shown in Figure 6d, the WVP value of PLA was $10.38 \times 10^{-3}$ g $d^{-1}$ $m^{-1}$ $kPa^{-1}$. After adding 1% CNC and MCNC, the WVP values of the films reduced to $10.24 \times 10^{-3}$ g $d^{-1}$ $m^{-1}$ $kPa^{-1}$ and $10.19 \times 10^{-3}$ g $d^{-1}$ $m^{-1}$ $kPa^{-1}$, respectively. This may be due to the gap in the film being filled by a uniform distribution of CNC and MCNC. At this point, the film structure became denser, making it more difficult for water vapor to pass through. Overall, the addition of CNC and MCNC has no significant effect on the WVP value of PLA films ($p > 0.05$).

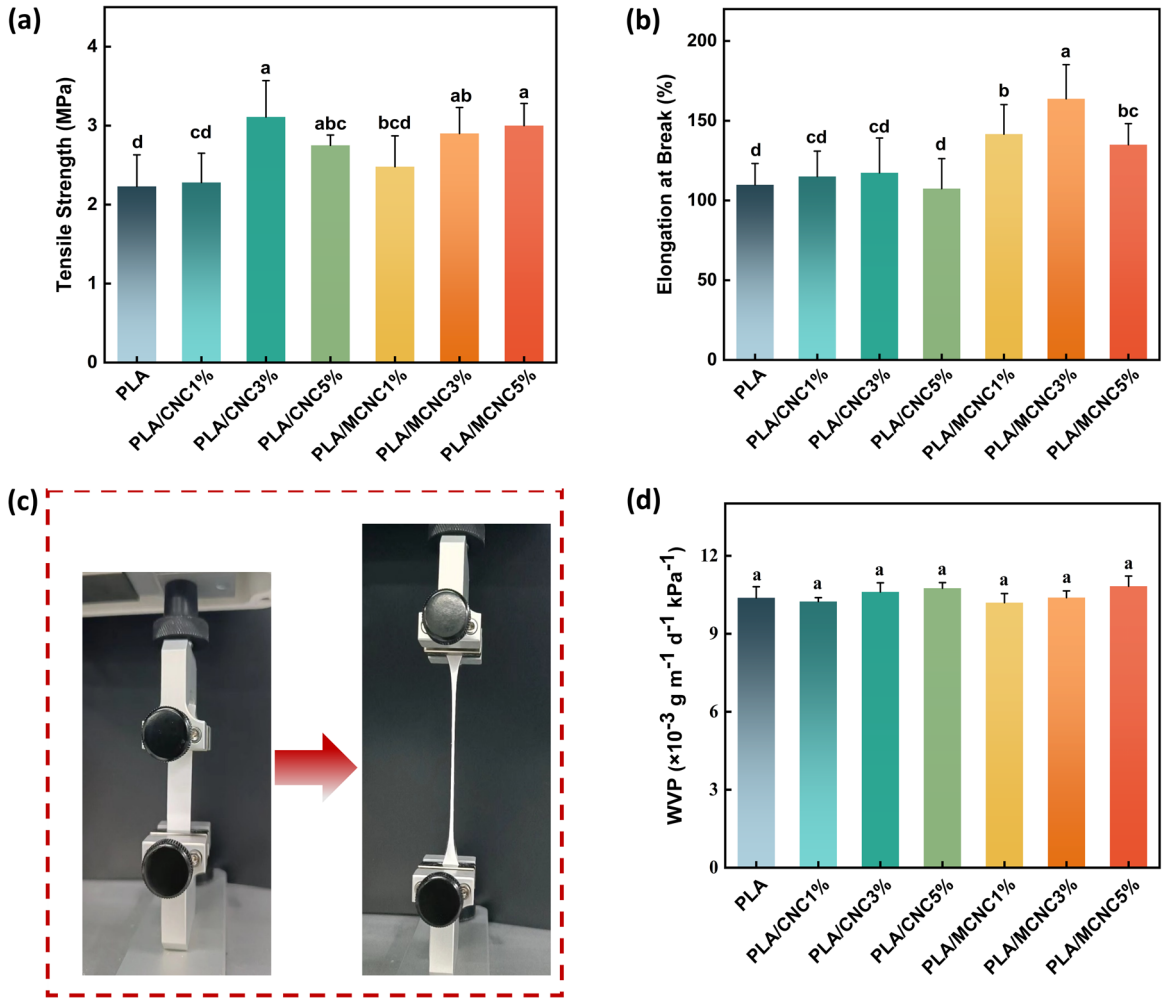


**FIGURE 6** | Tensile strength (a), elongation at break (b), physical diagram of the tensile testing process before and after stretching (c), and WVP of the nanofiber films (d).

Figure 7 presents the WCA measurements for three different nanofiber films: pure PLA, PLA/CNC3%, and PLA/MCNC3%. The graph demonstrated that all nanofiber films displayed a hydrophobic surface (> 90°). The WCA decreased with the extension of time, potentially due to the porous network structure of the nanofiber films, which facilitated the permeation of water droplets into the films. The WCA of the PLA film was 107.89°, which was consistent with the findings reported by Li et al. (2022). The incorporation of CNC had no significant impact on the WCA of the PLA film ($p < 0.05$). In the PLA/MCNC3% film, the addition of MCNC increases the WCA value, indicating that the hydrophobicity of the film was enhanced.

### 3.7 | Antioxidant Properties Analysis

The antioxidant capacity of nanofiber films was evaluated through DPPH and ABTS free radical scavenging abilities. As depicted in Figure 8, PMK0 nanofiber films barely exhibit antioxidant capacity. When the addition amount of kaempferol was 5%, the DPPH and ABTS free radical scavenging abilities were significantly enhanced ($p < 0.05$), higher than those of PMK0 nanofiber films. With the increase in the addition amount of kaempferol, the DPPH and ABTS free radical scavenging rates significantly increase to 92.19% and 96.72%, respectively. This result indicates that kaempferol can significantly enhance the antioxidant activity of the films. This enhancement effect was mainly attributed to the plentiful phenolic hydroxyl groups present in kaempferol molecules. These groups can impede free radical chain reactions by means of the electron-proton transfer mechanism (Sheng et al. 2025). Therefore, PMK nanofiber films have the potential to inhibit food oxidation when applied in food packaging.

## 4 | Conclusion

In this study, the composite nanofiber film composed of PLA and MCNC exhibits remarkable thermal stability, water resistance, and mechanical properties. FTIR analysis confirmed the successful introduction of the ester bond within MCNC. The TG analysis, mechanical assessments, and contact angle measurements demonstrate that incorporating MCNC enhances the thermal properties of the PLA film, resulting in an increase in thermal degradation temperature by 19°C and significantly improving the mechanical properties and water resistance of the PLA film. The TS, EAB, and contact angle exhibited

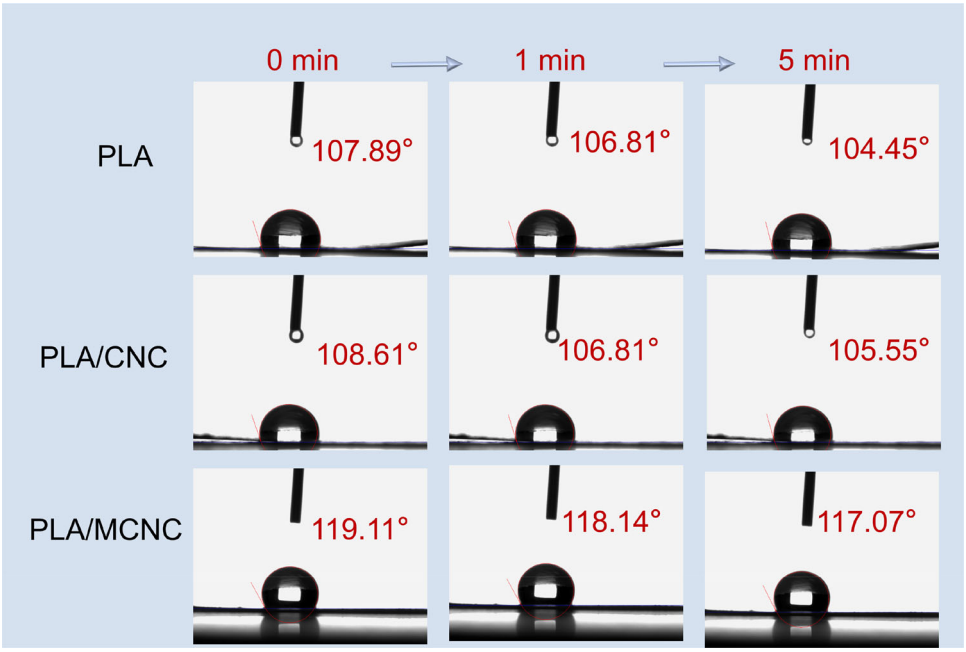


**FIGURE 7** | Water contact angle of different nanofiber films.

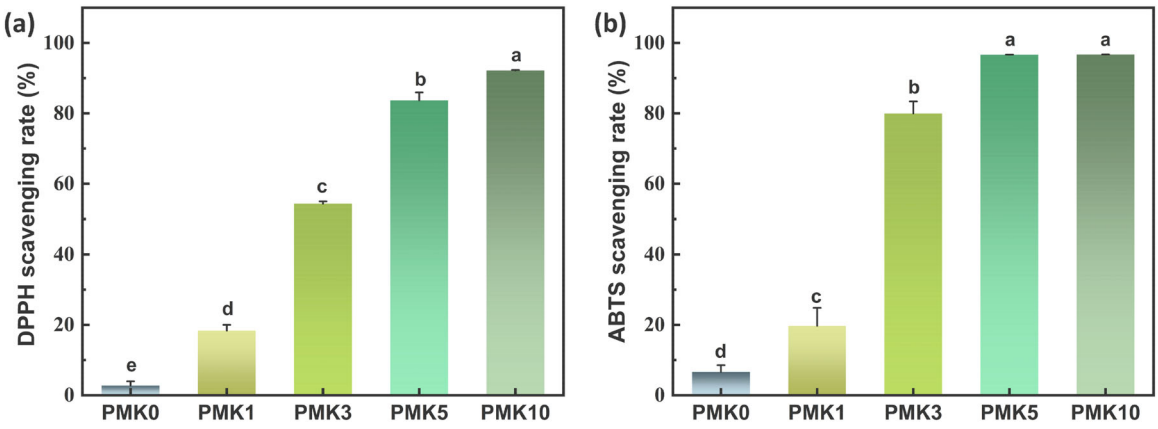


**FIGURE 8** | DPPH (a) and ABTS (b) scavenging rates of the nanofiber films with different kaempferol contents.

increases of 30.04%, 49.11%, and 11.22°, respectively. Furthermore, the addition of kaempferol imparted higher antioxidant capacity to the PMK nanofiber film. In conclusion, the PLA/MCNC composite developed in this study exhibits significant potential for application in high-performance active nanofiber films, thereby broadening the use of biodegradable PLA composites in food packaging and other industries.

### Author Contributions

**Chaoqiao Zhu:** writing–original draft, software, methodology, investigation, formal analysis, data curation. **Ming Tian:** investigation, methodology, **Dequan Zhang:** writing–review and editing, project administration, funding acquisition. **Qingfeng Yang:** formal analysis, data curation, writing–review and editing. **Debao Wang:** formal analysis, data curation. **Simin Fan:** software, methodology. **Xin Li:** project administration. **Wei Yang:** resources, project administration. **Chengli Hou:** writing–review and editing, project administration, funding acquisition.

### Acknowledgments

The authors are grateful to Mrs.Yanli Sun and Mrs. Ying Wang of Electron Microscope Center as well as Mrs. Chunhong Li of National Key Laboratory of Argo-products Processing, Institute of Food Science and Technology, Chinese Academy of Agricultural Science for providing technical support. This work was supported by the Major Science and Technology Project of Yunnan Province (No.202102AE090039).

### Ethics Statement

The authors have nothing to report.

### Conflicts of Interest

The authors declare no conflicts of interest.

### Data Availability Statement

The data that support the findings of this study are available on request from the corresponding author. The data are not publicly available due to privacy or ethical restrictions.

## References


Azka, M. A., S. M. Sapuan, H. Abral, E. S. Zainudin, and F. A. Aziz. 2024. "An Examination of Recent Research of Water Absorption Behavior of Natural Fiber Reinforced Polylactic Acid (PLA) Composites: A Review." *International Journal of Biological Macromolecules* 268: 131845. https://doi.org/10.1016/j.ijbiomac.2024.131845.

Chaturvedi, S., A. Kataria, V. Chaudhary, et al. 2023. "Bionanocomposites Reinforced With Cellulose Fibers and Agro-Industrial Wastes." In *Cellulose Fibre Reinforced Composites*, edited by R. ArunRamnath, M. R. Sanjay, S. Siengchin, and V. Fiore, 317–342. Woodhead Publishing. https://doi.org/10.1016/B978-0-323-90125-3.00017-3.

Cheran, E., C. Sharmila Rahale, P. Divyabharathi, C. Viswanathan, and L. Narayanan. 2024. "Corn Cob Nanocellulose Packaging for Increasing the Shelf Life of Food Products." *International Journal of Biological Macromolecules* 268: 131403. https://doi.org/10.1016/j.ijbiomac.2024.131403.

Dhali, K., F. Daver, P. Cass, and B. Adhikari. 2022. "Surface Modification of the Cellulose Nanocrystals Through Vinyl Silane Grafting." *International Journal of Biological Macromolecules* 200: 397–408. https://doi.org/10.1016/j.ijbiomac.2022.01.079.

Dhar, P., D. Tarafder, A. Kumar, and V. Katiyar. 2016. "Thermally Recyclable Polylactic Acid/Cellulose Nanocrystal Films Through Reactive Extrusion Process." *Polymer* 87: 268–282. https://doi.org/10.1016/j.polymer.2016.02.004.

Ertan, K., A. Celebioglu, R. Chowdhury, et al. 2023. "Carvacrol/Cyclodextrin Inclusion Complex Loaded Gelatin/Pullulan Nanofibers for Active Food Packaging Applications." *Food Hydrocolloids* 142: 108864. https://doi.org/10.1016/j.foodhyd.2023.108864.

Etale, A., A. J. Onyianta, J.-C. Eloi, J. Rowlandson, and S. J. Eichhorn. 2024. "Phosphorylated Cellulose Nanocrystals: Optimizing Production by Decoupling Hydrolysis and Surface Modification." *Carbohydrate Polymers* 325: 121560. https://doi.org/10.1016/j.carbpol.2023.121560.

Fan, S., D. Wang, X. Wen, et al. 2023. "Incorporation of Cinnamon Essential Oil-Loaded Pickering Emulsion for Improving Antimicrobial Properties and Control Release of Chitosan/Gelatin Films." *Food Hydrocolloids* 138: 108438. https://doi.org/10.1016/j.foodhyd.2022.108438.

Gao, C., P. Chen, Y. Ma, et al. 2023. "Multifunctional Polylactic Acid Biocomposite Film for Active Food Packaging With UV Resistance, Antioxidant and Antibacterial Properties." *International Journal of Biological Macromolecules* 253: 126494. https://doi.org/10.1016/j.ijbiomac.2023.126494.

Gazquez-Navarro, J. J., J. Ivorra-Martinez, L. Sanchez-Nacher, D. Garcia-Garcia, and J. Gomez-Caturla. 2024. "New Tartrate and α-Tocopherol Based Environmentally Friendly Plasticizers for Improvement of the Ductility of Polylactic Acid." *Polymer* 308: 127361. https://doi.org/10.1016/j.polymer.2024.127361.

Gulzar, S., M. Tagrida, K. Nilsuwan, T. Prodpran, and S. Benjakul. 2022. "Electrospinning of Gelatin/Chitosan Nanofibers Incorporated With Tannic Acid and Chitooligosaccharides on Polylactic Acid Film: Characteristics and Bioactivities." *Food Hydrocolloids* 133: 107916. https://doi.org/10.1016/j.foodhyd.2022.107916.

Huang, S., S. Zou, and Y. Wang. 2023. "Construction of Compostable Packaging With Antibacterial Property and Improved Performance Using Sprayed Coatings of Modified Cellulose Nanocrystals." *Carbohydrate Polymers* 305: 120539. https://doi.org/10.1016/j.carbpol.2023.120539.

Karimi Sani, I., M. Masoudpour-Behabadi, M. Alizadeh Sani, et al. 2023. "Value-Added Utilization of Fruit and Vegetable Processing by-Products for the Manufacture of Biodegradable Food Packaging Films." *Food Chemistry* 405: 134964. https://doi.org/10.1016/j.foodchem.2022.134964.

Kataria, A., S. Chaturvedi, V. Chaudhary, et al. 2023. "Cellulose Fiber-Reinforced Composites—History of Evolution, Chemistry, and Structure." In *Cellulose Fibre Reinforced Composites*, edited by R. ArunRamnath, M. R. Sanjay, S. Siengchin, and V. Fiore, 1–22. Woodhead Publishing. https://doi.org/10.1016/B978-0-323-90125-3.00012-4.

Khanjanzadeh, H., R. Behrooz, N. Bahramifar, et al. 2018. "Surface Chemical Functionalization of Cellulose Nanocrystals by 3-Aminopropyltriethoxysilane." *International Journal of Biological Macromolecules* 106: 1288–1296. https://doi.org/10.1016/j.ijbiomac.2017.08.136.

Li, M., L. Guo, Y. Mu, et al. 2024. "Gelatin Films Reinforced by Tannin-Nanocellulose Microgel With Improved Mechanical and Barrier Properties for Sustainable Active Food Packaging." *Food Hydrocolloids* 149: 109642. https://doi.org/10.1016/j.foodhyd.2023.109642.

Li, S., X. Liu, X. Zhang, et al. 2024. "Preparation and Characterization of Zein-Tannic Acid Nanoparticles/Chitosan Composite Films and Application in the Preservation of Sugar Oranges." *Food Chemistry* 437: 137673. https://doi.org/10.1016/j.foodchem.2023.137673.

Li, W., W. Sun, L. Jia, et al. 2022. "Poly-L-Lactic Acid (Plla)/Anthocyanin Nanofiber Color Indicator Film for Headspace Detection of Low-Level Bacterial Concentration." *International Journal of Biological Macromolecules* 215: 123–131. https://doi.org/10.1016/j.ijbiomac.2022.06.034.

Liao, M., X. Jian, Y. Zhao, et al. 2023. "Sandwich-Like" Structure Electrostatic Spun Micro/Nanofiber Polylactic Acid-Polyvinyl Alcohol-Polylactic Acid Film Dressing With Metformin Hydrochloride and Puerarin for Enhanced Diabetic Wound Healing." *International Journal of Biological Macromolecules* 253: 127223. https://doi.org/10.1016/j.ijbiomac.2023.127223.

Lin, D., Y. Li, Y. Huang, et al. 2022. "Properties of Polyvinyl Alcohol Films Reinforced by Citric Acid Modified Cellulose Nanocrystals and Silica Aerogels." *Carbohydrate Polymers* 298: 120116. https://doi.org/10.1016/j.carbpol.2022.120116.

Lin, N., and A. Dufresne. 2014. "Surface Chemistry, Morphological Analysis and Properties of Cellulose Nanocrystals With Gradiented Sulfation Degrees." *Nanoscale* 6, no. 10: 5384–5393. https://doi.org/10.1039/C3NR06761K.

Lin, N., J. Huang, P. R. Chang, J. Feng, and J. Yu. 2011. "Surface Acetylation of Cellulose Nanocrystal and Its Reinforcing Function in Poly(Lactic Acid)." *Carbohydrate Polymers* 83, no. 4: 1834–1842. https://doi.org/10.1016/j.carbpol.2010.10.047.

Liu, Y., X. Xu, M. Gao, et al. 2024. "Nanocellulose-Based Functional Materials for Physical, Chemical, and Biological Sensing: A Review of Materials, Properties, and Perspectives." *Industrial Crops and Products* 212: 118326. https://doi.org/10.1016/j.indcrop.2024.118326.

Malbos, L. B., M. L. Iglesias-Montes, I. T. Seoane, V. P. Cyras, and L. B. Manfredi. 2024. "Biobased Ternary Composites for Food Packaging: Influence of Natural Plasticizers and Starch on Polylactic Acid Performance." *Journal of Materials Science* 59: 20304–20324. https://doi.org/10.1007/s10853-024-10375-3.

Mo, J., Y. Wang, J. Wang, et al. 2022. "Hydrophobic/Oleophilic Polylactic Acid Electrospun Fibrous Membranes With the Silicone Semi-Interpenetrated Networks for Oil–Water Separation." *Journal of Materials Science* 57, no. 33: 16048–16063. https://doi.org/10.1007/s10853-022-07634-6.

N'a, Z., F. M.s.a, T. I.s.m.a, B. M.s.m, and O. S.h. 2023. "Mechanical, Thermal and Antimicrobial Properties of Pla/Jackfruit Skin Composites Containing Thymol and Nanocellulose." *Materials Today: Proceedings*. In press. https://doi.org/10.1016/j.matpr.2023.01.397.

Niu, W., Y. Guo, W. Huang, et al. 2022. "Aliphatic Chains Grafted Cellulose Nanocrystals With Core-Corona Structures for Efficient Toughening of Pla Composites." *Carbohydrate Polymers* 285: 119200. https://doi.org/10.1016/j.carbpol.2022.119200.

Niu, X., Y. Liu, Y. Song, J. Han, and H. Pan. 2018. "Rosin Modified Cellulose Nanofiber as a Reinforcing and Co-Antimicrobial Agents in Polylactic Acid/Chitosan Composite Film for Food Packaging."

*Carbohydrate Polymers* 183: 102–109. https://doi.org/10.1016/j.carbpol.2017.11.079.

Ojogbo, E., C. Tzoganakis, and T. H. Mekonnen. 2025. "Silane-Modified Cellulose Nanocrystals (CNCs) Based Natural Rubber Composites." *Composites, Part A: Applied Science and Manufacturing* 190: 108632. https://doi.org/10.1016/j.compositesa.2024.108632.

Sheng, W., L. Yang, Y. Yang, C. Wang, G. Jiang, and Y. Tian. 2025. "Photo-Responsive Cu-Tannic Acid Nanoparticle-Mediated Antibacterial Film for Efficient Preservation of Strawberries." *Food Chemistry* 464: 141711. https://doi.org/10.1016/j.foodchem.2024.141711.

Sucinda, E. F., M. S. Abdul Majid, M. J. M. Ridzuan, E. M. Cheng, H. A. Alshahrani, and N. Mamat. 2021. "Development and Characterisation of Packaging Film From Napier Cellulose Nanowhisker Reinforced Polylactic Acid (Pla) Bionanocomposites." *International Journal of Biological Macromolecules* 187: 43–53. https://doi.org/10.1016/j.ijbiomac.2021.07.069.

Sung, S. H., Y. Chang, and J. Han. 2017. "Development of Polylactic Acid Nanocomposite Films Reinforced With Cellulose Nanocrystals Derived From Coffee Silverskin." *Carbohydrate Polymers* 169: 495–503. https://doi.org/10.1016/j.carbpol.2017.04.037.

Thompson, L., M. Nikzad, I. Sbarski, and A. Yu. 2022. "Esterified Cellulose Nanocrystals for Reinforced Epoxy Nanocomposites." *Progress in Natural Science: Materials International* 32, no. 3: 328–333. https://doi.org/10.1016/j.pnsc.2022.05.001.

Wahlström, N., M. S. Hedenqvist, and F. Vilaplana. 2024. "Citric Acid Tailors the Mechanical and Barrier Properties of Arabinoxylan-Gluten Crosslinked Glycoprotein Films." *Food Hydrocolloids* 153: 110012. https://doi.org/10.1016/j.foodhyd.2024.110012.

Wu, H., T. Li, L. Peng, et al. 2023. "Development and Characterization of Antioxidant Composite Films Based on Starch and Gelatin Incorporating Resveratrol Fabricated by Extrusion Compression Moulding." *Food Hydrocolloids* 139: 108509. https://doi.org/10.1016/j.foodhyd.2023.108509.

Yanat, M., M. Muthurajan, M. Strubel, K. Grolle, and K. Schroën. 2023. "Polylactic Acid Films Reinforced With Chitin Nanocrystals: Biodegradation and Migration Behavior." *Food Packaging and Shelf Life* 40: 101217. https://doi.org/10.1016/j.fpsl.2023.101217.

Yang, S., C. Chen, W. Li, and S. Liu. 2023. "Study on the Effect of 5/20 and 20/80°C Temperature Cycle Curing Regimes on the Properties of Polyacrylate Dispersion-Modified Cement Mortar." *Construction and Building Materials* 399: 132520. https://doi.org/10.1016/j.conbuildmat.2023.132520.

Yun, Y., W. Liu, Y. Ning, J. Li, and L. Wang. 2024. "Fabricating a High-Loading Smart Film to Monitor Pork Freshness via Adsorption of Anthocyanins on Simultaneously Etched, Anionized and Bleached Wood Cell Wall." *Food Chemistry* 460: 140485. https://doi.org/10.1016/j.foodchem.2024.140485.

Zhou, L., K. Ke, M.-B. Yang, and W. Yang. 2021. "Recent Progress on Chemical Modification of Cellulose for High Mechanical-Performance Poly(Lactic Acid)/Cellulose Composite: A Review." *Composites Communications* 23: 100548. https://doi.org/10.1016/j.coco.2020.100548.

Zhu, Z., M. Yu, R. Ren, H. Wang, and B. Kong. 2024. "Thymol Incorporation Within Chitosan/Polyethylene Oxide Nanofibers by Concurrent Coaxial Electrospinning and In-Situ Crosslinking From Core-Out for Active Antibacterial Packaging." *Carbohydrate Polymers* 323: 121381. https://doi.org/10.1016/j.carbpol.2023.121381.

## Supporting Information

Additional supporting information can be found online in the Supporting Information section.